PHYSICAL REVIEW B **69**, 020102(R) (2004)

Crystal-melt interfacial free energies in metals: fcc versus bcc

D. Y. Sun,[1,*] M. Asta,[1] J. J. Hoyt,[2] M. I. Mendelev,[3] and D. J. Srolovitz[3]
[1]*Department of Materials Science and Engineering, Northwestern University, Evanston, Illinos 60208, USA*
[2]*Sandia National Laboratories, MS 1411, Albuquerque, New Mexico 87185, USA*
[3]*Princeton Materials Institute, Department of Mechanical and Aerospace Engineering, Princeton University, Princeton, New Jersey 08544, USA*
(Received 20 October 2003; published 23 January 2004)

The structural dependence of crystal-melt interfacial free energies (γ) is investigated for fcc and bcc solids through molecular-dynamics calculations employing interatomic potentials for Fe. We compute $\approx$30–35 % lower values of γ for the bcc structure, and find that our results cannot be explained simply in terms of differences in latent heats (L) or densities (ρ) for bulk bcc and fcc phases. We observe a strong structural dependence of the Turnbull coefficient $\alpha = \gamma / L\rho^{2/3}$, and find a trend towards lower crystalline anisotropies of γ for the bcc structure relative to fcc.

DOI: 10.1103/PhysRevB.69.020102 PACS number(s): 64.70.Dv, 68.08.De

In deeply undercooled melts crystallization frequently proceeds through the nucleation of metastable phases. A widely studied example involves the formation of metastable bcc structures in systems with stable fcc solids. This phenomenon has been observed experimentally in a number of metal-alloy systems (e.g., Refs. 1–8) and in simulations for weakly charged colloids.[9] bcc order also has been observed within subcritical crystalline nuclei and at crystal-melt interfaces in numerical simulations[10] and density-functional-theory (DFT) calculations[11] for the Lennard-Jones system, although such order is relatively absent for the hard sphere (HS) system.[12,13] Metastable crystallization of bcc solids is generally attributed to a lower value of the solid-liquid interfacial free energy (γ) relative to fcc, resulting in a reduced barrier for nucleation from the melt. The origins of such crystal-structure dependencies for γ are typically discussed within the framework of the scaling relation proposed by Turnbull[14]:

$$\gamma = \alpha T \Delta S_f \rho^{2/3}, \tag{1}$$

where T is temperature, ΔS_f the entropy of fusion, ρ is the solid atomic density, and α is the so-called Turnbull coefficient. From Eq. (1), structural variatons in γ can be associated with changes in bulk properties (ΔS_f, ρ), and/or from explicit crystallographic dependencies reflected in the parameter α.

To date, relatively few direct calculations have been undertaken to explore the magnitude of crystal-structure dependencies in γ. Nucleation simulations for weakly charged colloids[9] and DFT calculations for adhesive hard spheres[15] yield values of γ for bcc that are 10–50 % lower than for fcc. Interestingly, in the DFT calculations for the HS system by Marr and Gast[15] identical values are obtained for the fcc and bcc Turnbull coefficients, and the lower values of γ_{bcc} are thus associated entirely with smaller values of ΔS_f for the bcc structure. This result differs qualitatively with a key prediction of the theoretical model due to Spaepen, Meyer, and Thompson (SMT) (Refs. 17–19) that has been employed widely in the interpretation of metastable bcc crystallization data for fcc-based alloys. SMT derived expressions for γ employing a polytetrahedral model for the liquid structure to compute the excess configurational entropy of a melt in contact with a rigid solid, obtaining $\alpha = 0.86$ for fcc and $\alpha = 0.71$ for bcc. The SMT model thus predicts approximately 20% differences in the Turnbull coefficient for fcc and bcc structures, providing an appreciable source for the lowering of γ_{bcc} relative to γ_{fcc}, even for metallic systems where ΔS_f and ρ are similar for the two structures. While the SMT values for the overall magnitudes of α are known to be overestimates for both the HS system[15,16,20] and fcc metals (e.g., Ref. 21), the prediction $\alpha_{bcc} \approx 0.82 \alpha_{fcc}$ has nevertheless been found to be consistent with numerous experimental observations related to metastable bcc crystallization in alloys; measured boundaries delineating primary crystallization of (stable) fcc and (metastable) bcc phases in Fe- and Ni-based alloy systems have been well reproduced[2–7] on the basis of classical nucleation theory employing the SMT model for the structural dependence of γ.

The present study is aimed at providing further insight into the dependence of solid-liquid interfacial free energies upon crystal structure in metals with competing fcc and bcc phases. We employ direct molecular-dynamics (MD) calculations of γ for fcc and bcc based upon recently developed interatomic-potential models for Fe.[22,23] Calculated values of γ for bcc are roughly 30–35 % lower than those for fcc. We derive $\alpha_{bcc} \approx 0.65 \alpha_{fcc}$, providing direct evidence in support of a significant crystal-structure dependence of the Turnbull coefficient in metal systems with competing fcc and bcc phases.

MD calculations are based upon two different many-body potentials for Fe developed by Ackland *et al.*[22] and Mendelev *et al.*[23] Hereafter these potentials will be referred to by the initials of the authors: *ABCH* (Ref. 22) and $MH(SA)^2$.[23] Both potentials are of the ''pair-functional'' form (e.g., Ref. 24) common to the embedded-atom model[25] (EAM) and second-moment tight-binding model. The *ABCH* potential was derived by fitting to static properties of bcc Fe at zero temperature, whereas $MH(SA)^2$ also incorporates interatomic force information for the liquid derived from *ab initio* calculations. The latter potential leads to a much better agreement with experimental measurements for liquid struc-

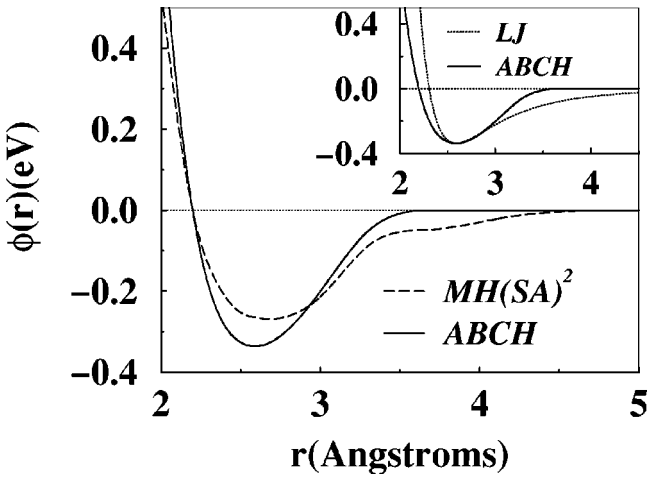

FIG. 1. Effective-pair potentials derived from the *ABCH* (solid line) and $MH(SA)^2$ (dashed line) many-body potentials for Fe. The inset compares the *ABCH* pair potential (solid line) with a Lennard-Jones (LJ) potential (dashed) having the same well depth and equilibrium interatomic separation.

ture factors and melting properties. We employ the *ABCH* potential to make direct comparisons between fcc and bcc crystal-melt interfacial properties, and use $MH(SA)^2$ to derive refined values for bcc interfaces. A comparison of results obtained with these different potential models provides a means for checking the sensitivity of our conclusions to details of the form of the interatomic interactions. To investigate the role of many-body interactions we repeat calculations for the *ABCH* model using an ''effective'' pair potential,[24] obtained by expanding the density dependence of the embedding function to second order. The resulting pair potential is shown in Fig. 1, where it is compared to a Lennard-Jones potential with the same equilibrium spacing and well depth; the *ABCH*-derived pair potential is significantly shorter in range and less repulsive at short distances. Although it is not considered further in this study, we also show in Fig. 1 an effective pair potential derived analogously from the $MH(SA)^2$ EAM model; a comparison between the *ABCH* and $MH(SA)^2$ curves illustrates the qualitative differences between these two potentials.

Solid-liquid interfacial free energies were calculated by MD employing the capillary fluctuation method (CFM).[21,26–29] Here we give a brief overview of the implementation of this method in the present calculations; further details will be provided in a future publication. The CFM is based upon an application of the relation between the equilibrium height-fluctuation spectrum of a rough crystal-melt interface and its *stiffness*: $\langle|A(k)|^2\rangle = k_B T/bW(\gamma+\gamma'')k^2$, where $A(k)$ is the Fourier transform of the interface height profile, and W and b (with $b \ll W$) denote the length and thickness of a thin (''ribbonlike'') crystal-melt boundary. $\gamma + \gamma''$ defines the stiffness, with γ'' denoting the second derivative of $\gamma(\hat{n})$ with respect to the angle of the local interface normal relative to its average orientation.

Application of the CFM begins by equilibrating periodic simulation cells with coexisting solid and liquid phases at the (zero-pressure) melting temperature. The present study makes use of simulation cells with typical cross-sectional dimensions of $W = 19$ nm and $b = 1.5$ nm, and periodic lengths normal to the solid-liquid interfaces approximately equal to $2W$. Instantaneous positions of the solid-liquid interfaces are sampled during (microcanonical) MD simulations employing the structural order parameter introduced by Hoyt *et al.*[26]: $\phi_i = 1/n\Sigma_j|\vec{r}_{ij} - \vec{r}_{ij}^{\,ideal}|^2$, where the sum is over the n nearest neighbors j of atom i, r_{ij} is the vector connecting sites i and j, and $\vec{r}_{ij}^{\,ideal}$ corresponds to the related positions in an ideal crystal. For systems with fcc structures the sum is over the $n = 12$ nearest neighbors, while for bcc systems it was found that including both first and second neighbors ($n = 14$) led to improved separation in the identification of solid and liquid atoms. With the use of the order parameter ϕ, instantaneous positions of the solid-liquid interface were identified and Fourier-transformed to derive $A(k,t)$ at intervals of 0.1 ps for simulations lasting several hundred ps. From this MD data, $\langle|A(k)|^2\rangle$ and associated statistical uncertainties were derived as described in Ref. 27. Interface stiffnesses were then extracted from the slope of the (weighted-least-squares) fit of $\langle|A(k)|^2\rangle$ vs $1/k^2$ using data for k ranging between zero and 0.22 Å^{-1}.

TABLE I. Interface stiffnesses for bcc Fe calculated with the *ABCH* potential. The first column gives interface orientations in the notation of Ref. 26. Calculated stiffnesses are in the second column where numbers in parentheses denote 95% confidence intervals in the final significant figure(s). Stiffness values in columns 3 and 4 are computed from Eq. (2) with parameters derived by fitting, respectively, to data for all six orientations and to only the first three.

Orientation	Calculated stiffness (mJ/m^2)	Fit 1 (mJ/m^2)	Fit 2 (mJ/m^2)
001[010]	196 (16)	192	196
$1\bar{1}0$[001]	198 (14)	199	198
$1\bar{1}0$[110]	218 (13)	218	218
111[$1\bar{1}0$]	213 (21)	215	216
120[001]	193 (4)	193	197
120[$2\bar{1}0$]	209 (12)	209	210

Once the stiffnesses have been calculated for a number of crystallographic orientations, interfacial free energies and their associated crystalline anisotropies are extracted using a cubic-harmonic expansion of the form

$$\gamma(\hat{n})/\gamma_0 = 1 + \epsilon_1\left(\sum_{i=1}^{3} n_i^4 - \frac{3}{5}\right) + \epsilon_2\left(3\sum_{i=1}^{3} n_i^4 + 66 n_1^2 n_2^2 n_3^2 - \frac{17}{7}\right), \qquad (2)$$

where γ_0 denotes the spherically averaged value of the interfacial free energy, ϵ_1 and ϵ_2 are anisotropy parameters, and n_i denote the components of the interface normal. In previous work it has been shown that Eq. (2) provides an accurate parameterization of the orientation dependence of γ for a variety of fcc-based systems.[26,28,29] In the present study, which represents the first application of the CFM to a non-

TABLE II. Calculated melting and solid-liquid interfacial properties for FCC and BCC structures based upon the *ABCH*, $MH(SA)^2$ and *ABCH*-effective-pair (pair) potentials. Numbers in parentheses denote 95% confidence intervals in the final significant figure(s).

Potential:	*ABCH*	*ABCH*	Pair	Pair	$MH(SA)^2$
Structure:	BCC	FCC	BCC	FCC	BCC
T_M (K)	2358	2236	2306	2215	1772
L (eV/atom)	0.218	0.200	0.259	0.212	0.162
γ_0 (mJ/m^2)	206(10)	319(12)	221(14)	311(14)	175(11)
α	0.32(2)	0.55(2)	0.29(2)	0.50(2)	0.36(2)
$\frac{\gamma_{100}-\gamma_{110}}{2\gamma_0}$ (%)	0.4(4)	2.8(4)	0.5(5)	2.4(4)	1.0(6)
$\frac{\gamma_{100}-\gamma_{111}}{2\gamma_0}$ (%)	0.5(4)	3.9(4)	0.4(6)	3.4(5)	1(2)

fcc-based structure, we have confirmed that Eq. (2) also accurately describes the orientation dependence of $\gamma(\hat{n})$ for the bcc crystals considered. In Table I we present results of directly calculated stiffness values for bcc interfaces derived from the *ABCH* potential, along with values extracted from fits of Eq. (2). The third column in Table I gives results of a fit of Eq. (2) to all six data points, while the numbers in the fourth column are based on a similar fit using only the three stiffnesses for {100} and {110} interfaces. The calculated stiffnesses are seen to be accurately reproduced (within estimated statistical uncertainties), even for the second fit where results for {111} and {210} interfaces represent predictions. This finding is similar to that of Hoyt *et al.*[26] who found that stiffnesses for {100} and {110} interfaces were sufficient to parametrize the full orientation dependence of $\gamma(\hat{n})$ for fcc Ni. In the following, all quoted γ values are derived in this way, fitting Eq. (2) to three calculated stiffnesses, with the exception of the bcc results for the *ABCH* potential which are based on the data for all six orientations given in Table I.

The third and fourth rows of Table II give the main results of the present study, listing calculated values of crystal-melt interfacial free energies (γ_0) and Turnbull coefficients (α) for fcc and bcc crystal structures. For a given crystal structure (fcc or bcc), the significant variations in the calculated γ_0 values (in particular between the *ABCH* and $MH(SA)^2$ potentials) reflect primarily differences in predicted melting temperatures; values of α for a given crystal structure are in much better agreement between potentials. For the *ABCH* many-body and effective-pair potentials both fcc and bcc structures are (meta)stable at their equilibrium melting temperatures. These models thus allow direct comparisons between the properties of the fcc and bcc crystal-melt interfaces derived from the same potential. With both potentials the values of γ_{bcc} are calculated to be lower than γ_{fcc} by 30–35 %, while values for the melting temperatures (T_M), ΔS_f and ρ differ only slightly between fcc and bcc structures. *The large differences in the calculated values of* γ_{fcc} *and* γ_{bcc} *are thus found to be associated primarily with an explicit dependence of the Turnbull coefficient upon crystal structure.*

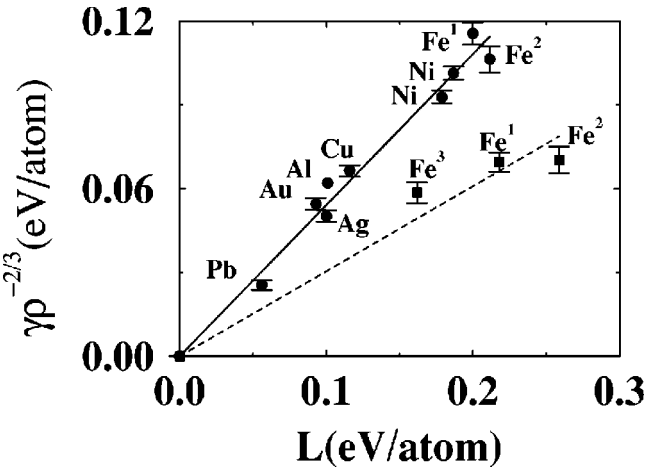

FIG. 2. Normalized interfacial free energies ($\hat{\gamma}$) vs latent heat (L) from calculations for EAM metals. The circles denote the fcc data, while the squares are for bcc. With the exception of the present data for Fe, results are obtained from Refs. 21 and 28, Fe^1 and Fe^2 denote results from the *ABCH* many-body and pair potentials, respectively, while Fe^3 corresponds to $MH(SA)^2$. Solid and dashed lines represent best fits through the fcc and bcc data, respectively.

Two additional features of the results in Table II warrant further discussion. First, the many-body and effective-pair forms of the *ABCH* potential show relatively minor differences in the calculated values of γ_0 and associated anisotropies. This suggests that many-body contributions to the interatomic interactions have a relatively small effect on the calculated crystal-melt interfacial properties in metals. Furthermore, the *ABCH* results in the final two rows show substantially lower anisotropies in γ for bcc relative to fcc. Interestingly, equilibrium crystal-shape measurements[30,31] for the transparent organic materials succinonitrile (SCN) and pivalic acid (PVA), yield fourfold anisotropies for γ that are a factor of 5–10 lower for the bcc SCN structure relative to fcc PVA. While further data is needed to confirm this trend, these results combined with those of the current study suggest a tendency towards reduced anisotropy in γ for bcc relative to fcc crystal structures.

Figure 2 shows a comparison between the present results for fcc and bcc Fe, and previous calculations for fcc based EAM metals.[21,28] In this plot of $\hat{\gamma}=\gamma_0\rho^{-2/3}$ vs latent heat ($L=T_M\Delta S_f$) the Turnbull coefficient is given by the slope of the solid and dashed lines representing least-squares fits to the fcc and bcc results, respectively. The present results for fcc Fe are seen to be consistent with previous calculations for other fcc-based EAM systems. The best fit line for the fcc data corresponds to a Turnbull coefficient of $\alpha_{fcc}=0.54(2)$. As discussed in Ref. 21, this value is in good agreement with previous analyses of experimental measurements for elemental fcc metals, and it is very close to the value of $\alpha=0.51$ calculated for the HS system.[16,20] The three different bcc results derived in the present study are found to

obey the Turnbull scaling relation quite well. A fit to all three bcc results yields a value of $\alpha_{bcc}=0.32(3)$ while fitting only to the two results for the many-body potentials yields $\alpha_{bcc}=0.34(2)$. These estimates are 30–35 % lower than our calculated α_{fcc}.

Experimental estimates of γ for Fe have been derived from several maximum undercooling measurements.[14,32,33] Due to the large variation in reported maximum undercoolings, estimated values of α for Fe vary between roughly 0.44 and 0.57.[33] Our present results for fcc Fe are within this range, while those for bcc Fe fall somewhat below. Since a quantitative comparison with experiment remains problematic, we wish to emphasize instead our observation of a clear tendency towards the lowering of α and γ anisotropy going from fcc to bcc. These trends are found to be relatively insensitive to the detailed form of the interatomic potentials employed in this work. Very recently, the same trends have been observed by Davidchack and Laird[34] for the repulsive $1/r^6$ potential, which gives rise to (meta)stable bcc and fcc solid phases with very small bulk free-energy differences. Interestingly, the repulsive part of the *ABCH* pair potential in Fig. 1 is found to be well modeled by a $1/r^6$ form. The present results and those of Davidchack and Laird combined suggest that the tendencies towards lower values of α and γ anisotropy for bcc relative to fcc are general trends for systems where these two solid phases are competitive.

This research was supported by the U. S. Department of Energy, Office of Basic Energy Sciences, under Contract Nos. DE-FG02-01ER45910 (DYS, MA and JJH) and DE-FG02-99ER45797 (MIM and DJS), as well as the DOE Computational Materials Science Network program. Use was made of resources at the National Energy Research Scientific Computing Center, which is supported by the Office of Science of the Department of Energy under Contract No. DE-AC03-76SF00098. We are grateful to Profs. A. Karma and B. B. Laird for numerous helpful discussions, and to Dr. L. Gránásy for sharing with us his unpublished analysis cited in Ref. 33.

*Permanent address: Institute of Solid State Physics, Academia Sinica, 230031-Hefei, China.

[1] R.E. Cech, Trans. AIME J. Met. **206**, 535 (1956).
[2] G. Ghosh, Mater. Sci. Eng., A **189**, 277 (1994).
[3] T. Volkmann *et al.*, Metall. Mater. Trans. A **28**, 453 (1997).
[4] A. Zambon *et al.*, Acta Mater. **46**, 4657 (1998).
[5] M. Li *et al.*, Mater. Sci. Eng., A **268**, 90 (1999).
[6] D.M. Herlach, J. Phys.: Condens. Matter **13**, 7737 (2001).
[7] A.L. Greer and I.T. Walker, J. Non-Cryst. Solids **317**, 78 (2003).
[8] C. Notthoff *et al.*, Phys. Rev. Lett. **86**, 1038 (2001).
[9] S. Auer and D. Frenkel, J. Phys. C **14**, 7667 (2002).
[10] P.R. ten Wolde, M.J. Ruiz-Montero, and D. Frenkel, Phys. Rev. Lett. **75**, 2714 (1995).
[11] Y.C. Shen and D.W. Oxtoby, Phys. Rev. Lett. **77**, 3585 (1996).
[12] S. Auer and D. Frenkel, Nature (London) **409**, 1020 (2001).
[13] L. Gránásy and T. Pusztai, J. Chem. Phys. **117**, 10121 (2002).
[14] D. Turnbull, J. Appl. Phys. **21**, 1022 (1950).
[15] D.W. Marr and A.P. Gast, J. Chem. Phys. **99**, 2024 (1993).
[16] B.B. Laird, J. Chem. Phys. **115**, 2887 (2001).
[17] F. Spaepen, Acta Metall. **23**, 729 (1975).
[18] F. Spaepen and R.B. Meyer, Scr. Metall. **10**, 257 (1976).
[19] C. V. Thompson, Ph.D. thesis, Harvard University, 1979.
[20] R.L. Davidchack and B.B. Laird, Phys. Rev. Lett. **85**, 4751 (2000).
[21] J.J. Hoyt *et al.*, Mater. Sci. Eng., R. **41**, 121 (2003).
[22] G.J. Ackland, D.J. Bacon, A.F. Calder, and T. Harry, Philos. Mag. A **75**, 713 (1997).
[23] M. I. Mendelev, S. Han, D. J. Srolovitz, G. J. Ackland, D. Y. Sun, and M. Asta, Philos. Mag. **83**, 3977 (2003). We employ potential No. 2 reported in this manuscript.
[24] A.E. Carlsson, Solid State Phys. **43**, 1 (1990).
[25] M.S. Daw and M.I. Baskes, Phys. Rev. Lett. **50**, 1285 (1983); Phys. Rev. B **29**, 6443 (1984).
[26] J.J. Hoyt *et al.*, Phys. Rev. Lett. **86**, 5530 (2001).
[27] J.J. Hoyt and M. Asta, Phys. Rev. B **65**, 214106 (2002).
[28] J.R. Morris, Phys. Rev. B **66**, 144104 (2002).
[29] J.R. Morris and X.Y. Song, J. Chem. Phys. **119**, 3920 (2003).
[30] M. Muschol *et al.*, Phys. Rev. A **46**, 1038 (1992).
[31] M.E. Glicksman and N.B. Singh, J. Cryst. Growth **98**, 277 (1989).
[32] K.F. Kelton, Solid State Phys. **45**, 75 (1991).
[33] L. Gránásy (private communication).
[34] R. L. Davidchack and B. B. Laird (private communication).